Eur. Phys. J. A (2009)
DOI 10.1140/epja/i2008-10685-3

THE EUROPEAN PHYSICAL JOURNAL A

Regular Article – Theoretical Physics

Electric and magnetic response to the continuum for A = 7 isobars in a dicluster model

A. Mason, R. Chatterjee, L. Fortunato[a], and A. Vitturi

Dipartimento di Fisica "G. Galilei", Università di Padova and INFN, v. Marzolo 8, I-35131 Padova, Italy

Received: 19 June 2008 / Revised: 6 November 2008

Communicated by G. Orlandini

Abstract. The mirror isobars ^{7}Li and ^{7}Be are investigated in a dicluster model. The magnetic dipole moments and the magnetic dipole response to the continuum are calculated in this framework. The magnetic contribution is found to be small with respect to electric dipole and quadrupole excitations even at astrophysical energies, at a variance with the case of the deuteron. Energy-weighted molecular sum rules are evaluated and a formula for the molecular magnetic dipole sum rule is found which matches the numerical calculations. Cross-sections for photo-dissociation and radiative capture as well as the S-factor for reactions of astrophysical significance are calculated with good agreement with known experimental data.

PACS. 21.60.Gx Cluster models – 23.20.Js Multipole matrix elements – 25.60.Tv Radiative capture

1 Dicluster description of ^{7}Be and ^{7}Li

It is well known that the properties of $A = 7$ mass nuclei may be effectively described in terms of a dicluster model: two (inert) clusters in interaction with each other [1–8]. A long-standing description of these nuclei with such a dicluster picture has achieved excellent results and a continued interest because it catches the essential physics within a very simple, yet powerful, model. Such a simple nuclear-structure scheme may then be used in reaction calculations [9]. The need to go beyond this level of description may be justified only with the aim of taking into account more refined considerations on the role of the Pauli principle or on the occurrence of complex phenomena like polarization of the clusters, and not because the model itself does not reproduce static and dynamic properties of $A = 7$ nuclei to a good degree of accuracy. For example *ab initio* shell model calculations using a computationally heavy Monte Carlo method have successfully reproduced many properties of these and other light nuclei starting from a nucleon-nucleon interaction [10]. By computing ground-state overlap functions, these calculations have shown that ^{7}Be has a spectroscopic factor of almost 1 in the $\alpha + {}^3$He configuration and, similarly, ^{7}Li has a large spectroscopic factor in the $\alpha + t$ channel. A number of other approaches that we will not discuss here, such as Resonating Group Methods or Generator Coordinates Methods, are available to various degrees of complication and success. In addition we must mention a very recent study by Canton and Levchuk on the low-energy capture reactions [11] using the Multichannel Algebraic Scattering approach that has been applied to the $^3\mathrm{He}(\alpha,\gamma)^7\mathrm{Be}$ reaction at astrophysical energies achieving a good agreement with S-factors data.

We have shown in a recent paper [9] that the dicluster model may be profitably used to calculate a number of static and dynamic properties of ^{7}Li, especially in connection with excitations to the continuum in break-up processes. We apply here the same model to ^{7}Be and in addition we investigate the magnetic excitations to the continuum that were neglected in previous works. It is in fact important to give proper estimates of their contributions to reaction cross-sections, especially at energies of astrophysical interest. These two isospin mirrors not only display very similar ground-state properties, but also manifest a similar behaviour as long as their response to the continuum is considered. Nowadays it is becoming more and more evident that to properly describe structure and reactions of loosely bound systems, *e.g.* nuclei along the drip lines, it is essential to take into account the coupling to the continuum and the break-up channel. This is relatively simple in the case of one-particle halo nuclei. In the case of more complex weakly bound nuclei such as ^{7}Li or ^{7}Be, the cluster picture offers the possibility of describing the ground and a few excited states in terms formally analogous to that of a single-particle picture, with the *caveat* that the single particle is not just a neutron or a proton, but a composite one, like for instance a triton.

Of course, as in any theory driven by phenomenological considerations, a certain degree of approximation comes

[a] e-mail: fortunato@pd.infn.it

into play, and one needs to consider the pros and cons of the approach. We mention therefore that considering the clusters as spherical and elementary, but not point-like, has some implications: i) one neglects possible polarization effect, which may come into play because of the proximity of the two clusters and ii) one neglects nucleon exchange effects between the two clusters. We shall prove that these limitations are not severe (see also [9]) and the model works rather well for the $A = 7$ nuclei.

Our intercluster potential is assumed to be the sum of a nuclear Woods-Saxon potential, a Coulomb potential and a spin-orbit interaction:

$$V_{A_1-A_2} = V_{coul}(r) + V_{WS}(r) + V_{\boldsymbol{\ell}\cdot\boldsymbol{s}}(r). \qquad (1)$$

with $V_{\boldsymbol{\ell}\cdot\boldsymbol{s}}(r) = V_{\boldsymbol{\ell}\cdot\boldsymbol{s}}\boldsymbol{\ell}\cdot\boldsymbol{s}\frac{r_0^2}{r}\frac{\mathrm{d}V_{WS}(r)}{\mathrm{d}r}$. Here r_0 is the same radius parameter that enters into the parametrization of the Woods-Saxon potential, $\boldsymbol{\ell}$ and $\boldsymbol{s}$ are the orbital angular momentum and spin of the ^{3}H(^{3}He) cluster in ^{7}Li(^{7}Be) respectively. The Coulomb potential has the standard $1/r$ behaviour at large distances (point charge), but at small distances we use the Coulomb potential generated by a uniform spherical charge distribution.

Note that it is not possible to identify one of the two clusters as a core and the other as a valence particle, since the two fragments have comparable masses and charges. In the spin-orbit interaction, r_0 is the radius of the Woods-Saxon potential, $\boldsymbol{\ell}$ refers to the relative angular momentum, and $\boldsymbol{s}$ refers to the spin of the triton (helium-3) which can be seen as a "heavy" single particle for ^{7}Li (^{7}Be).

The $A = 7$ isobars are particularly challenging. They are weakly bound, but nevertheless they have one excited bound state. The low-lying response presents (as we will show) non-resonant as well as resonant peaks with comparable intensities. Aside from the importance in pure nuclear physics, the break-up, photo-dissociation and capture processes for these nuclei play an important role for astrophysics and for applicative purposes (*e.g.* lithium is used as coolant in nuclear reactors). We apply, in particular, our dicluster model to the calculation of astrophysical S-factors for the reaction ^{3}He$(\alpha,\gamma)^7$Be (and also ^{3}H$(\alpha,\gamma)^7$Li). Recently the LUNA Collaboration [12] has undergone a successful experimental campaign aimed at measuring the cross-section for this reaction which is thought to i) strongly influence the hydrogen-burning process in the Sun and consequently the solar neutrino production and ii) determine the primordial abundance of light elements which influences the determination of the baryon-to-photon ratio of the Universe from comparison with nucleosynthesis. In both these fields the determination of this quantity is crucial and this fact justifies even more the need for simple, but yet powerful, theories that could explain and reproduce the data. For a review of experiments in this direction see ref. [12].

The paper is organized as follows: the present section contains a summary of the method and deals with the parameters of the cluster-cluster potential and with the electromagnetic properties of the ^{7}Li and ^{7}Be systems. Static properties and transition rates among bound states are compared with data whenever possible. Section 2 contains a digression about molecular sum rules, their evaluation in the present case and the derivation of a new energy-weighted sum rule for magnetic dipole transitions, inspired to the Kurath single-particle sum rule [13,14]. Section 3 deals with the application to astrophysics and presents our results for the photo-dissociation and radiative capture reactions. In sect. 4 we present the S-factors for the two reactions ^{3}He$(\alpha,\gamma)^7$Be and ^{3}H$(\alpha,\gamma)^7$Li in comparison with known experimental measurements. The conclusions are followed by an appendix where a few useful formulae for dicluster nuclei are derived.

Table 1. Total magnetic moments (in μ_N) of ^{7}Be and ^{7}Li for different choices of relative angular momenta compared with the experimental value (last column). Even forgetting parity considerations that would of course leave only the $\ell = 1$ state as a possible candidate, it is clear that the best agreement is obtained in both cases by considering a relative p-wave.

	s	p	d	Exp.
^{7}Li	2.97	3.37	3.78	3.256427(2)
^{7}Be	−2.12	−1.53	−0.93	−1.398(15)

1.1 ^{7}Be

We consider ^{7}Be as formed by α and ^{3}He. The parameters of the cluster-cluster Woods-Saxon potential are $V_{WS} = -73.851$ MeV for the depth, 1.60 fm and 0.48 fm for its radius and diffusivity. The magnitude of the spin-orbit potential, $V_{\boldsymbol{\ell}\cdot\boldsymbol{s}} = 1.275$ MeV, is chosen in order to reproduce the splitting of the two bound eigenstates, respectively, at -1.58 and -0.98 MeV. The shape of the potential has been tuned in order to obtain an overall agreement with various observables, like the charge and mass radii. The α-particle has an intrinsic spin equal to zero, ^{3}He has spin 1/2 and the intercluster orbital angular momentum for the ground-state is $\ell = 1$: this can either be postulated on the basis of the Wildermuth connection [2] or it can be inferred phenomenologically, for example, from the magnetic moment for a dicluster nucleus. Using the intrinsic magnetic moment, masses and charges of the two clusters in formula (A.9) for the total magnetic moment, one can see from table 1 that the value that gives the best agreement is clearly $\ell = 1$ (which also gives the correct parity). Due to spin-orbit interaction the ground state has $j = 3/2^-$, while the first excited state has $j = 1/2^-$.

We calculate the relative motion wave function of the ground state, first excited state and continuum states by solving numerically the radial Schrödinger equation with the intercluster potential given in (1). In order to yield the resonant $7/2^-$ and $5/2^-$ states, we have to use a different set of parameters for the Woods-Saxon ($V_{WS} = -64.68$ MeV) and spin-orbit ($V_{\boldsymbol{\ell}\cdot\boldsymbol{s}} = 1.94$ MeV) potentials, but keeping the same geometry. With this choice we find that the width of the $f_{7/2}$ and $f_{5/2}$ resonances is in reasonable agreement with the experimental data (see table 2). A number of ground-state properties are found to be in good agreement with measured observables. We also calculate

Table 2. Static properties of ^{7}Be in a dicluster model and electromagnetic transition strengths between bound states. Definitions of some of these observables can be found in the appendix. Experimental values are taken from [15–17].

Quantity	This work	Experiments
$\langle r^2\rangle_{A+B}$ (fm)	2.48	2.48 ± 0.03
$\langle r^2\rangle^{ch}_{A+B}$ (fm)	2.52	2.52 ± 0.03
Q^{mat} (fm^2)	-11.83	–
Q^{ch} (fm^2)	-4.79	–
μ (μ_N)	-1.53	-1.398 ± 0.015
$B(E2, 3/2^- \to 1/2^-)$ (e^2fm^4)	18.3	–
$B(M1, 3/2^- \to 1/2^-)$ (μ^2)	1.86	1.87 ± 0.25
$\Gamma(7/2^-)$ (keV)	~ 90	175 ± 7
$\Gamma(5/2^-)$ (MeV)	~ 0.8	1.2

the $B(E2, 3/2^- \to 1/2^-)$ and $B(M1, 3/2^- \to 1/2^-)$ transition strengths between the ground state and the first excited bound state. All the calculated observables, obtained using the expressions given in appendix, are collected in table 2 with a comparison with known experimental data.

As has been done in ref. [9] for ^{7}Li, besides the quadrupole transition to the first excited bound state given in table 2, we also investigate the electromagnetic response of ^{7}Be to continuum states. Figure 1 shows the differential reduced transition probability (see ref. [18]), $\mathrm{d}B(E1)/\mathrm{d}E_c$, for continuum states allowed by an $E1$ transition. In this case there are no resonances in the low-lying continuum and the visible peaks have a non-resonant nature [19]. The dash-dotted line refers to the continuum $s_{1/2}$ state, the dashed and long-dashed lines refer to $d_{3/2}$ and $d_{5/2}$ states, respectively. The solid line gives the sum of all contributions. The total integrated non-energy weighted $B(E1)$ is $0.226\, e^2$fm^2 (see the next section for comments on sum rules).

Figure 2 shows the differential $\mathrm{d}B(E2)/\mathrm{d}E_c$ for continuum states allowed by an $E2$ transition. Long- and short-dashed lines refer to $f_{5/2}$ and $f_{7/2}$ states, respectively, while dot-dashed and dotted lines refer to $p_{1/2}$ and $p_{3/2}$ states, respectively. The f states take contributions both from the resonances and from the non-resonant part of the continuum, while the peaks of the p states arise purely from non-resonant transitions. We show also in the inset the full $f_{7/2}$-resonance on a different scale because it reaches a maximum of about $150\, e^2$fm^4/MeV. Finally the solid line gives the sum of all contributions. The total integrated non-energy weighted $B(E2)$ is $113.5\, e^2$fm^4 to be compared with the $B(E2, 3/2^- \to 1/2^-)$ value of $18.3\, e^2$fm^4. The non-resonant continuum states $p_{1/2}$ and $p_{3/2}$ are dominant at very low continuum energy, while they become negligible at higher energies around and beyond the $f_{5/2}$ peak.

In addition to electric excitations we also consider magnetic ones. Magnetic dipole interactions give normally contributions to the transition probabilities that are almost comparable with the electric quadrupole and smaller than the electric dipole. It appears however, already in

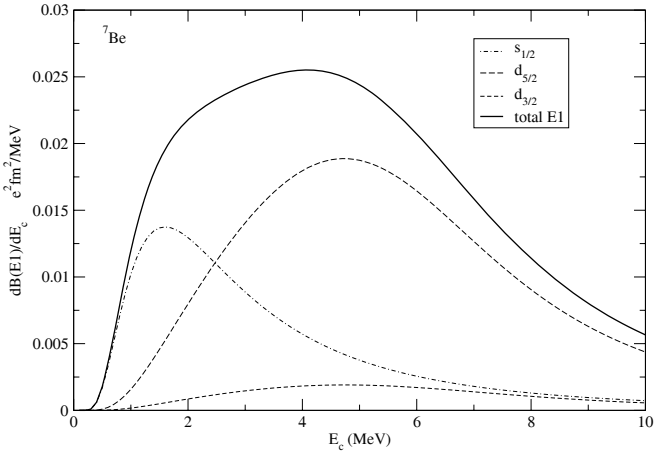

Fig. 1. Differential $\mathrm{d}B(E1)/\mathrm{d}E_c$ in e^2fm^2/MeV for transitions from the ground state to the continuum. Energies are in MeV, referred to the threshold for breaking into the α-^{3}He channel. Separated contributions are indicated in the legend. The solid line shows the sum of all the electric dipole contributions.

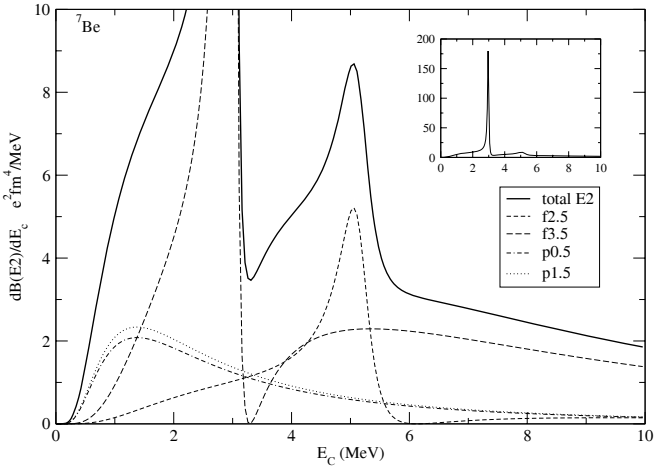

Fig. 2. Differential $\mathrm{d}B(E2)/\mathrm{d}E_c$ in e^2fm^4/MeV for transitions from the ground state to the continuum. Energies are in MeV, referred to the threshold for breaking into the α-^{3}He channel. Separated contributions are indicated in the legend. The solid line shows the sum of all the electric quadrupole contributions.

old calculations [20] for the photo-disintegration of the deuteron (the smallest dicluster nucleus), that they are relevant at astrophysical energies (say below 200 keV) where they even turn out to dominate over the electric dipole. For this reason we decided to investigate this theme to better understand the role they might play in low-energy nuclear reactions involving dicluster systems (cf. sect. 4).

The expression for the magnetic operator can be obtained from the multipoles expansions of the electromagnetic field with sources as (cf. ref. [21], chapt. 17):

$$M(M1) = \sum_i \left[\nabla(r_i^\lambda Y_\lambda(\theta,\phi))\right] \cdot \left[\frac{e^\lambda_{eff_i}\hbar}{m_i ec(\lambda+1)}\boldsymbol{\ell}_i + \frac{\mu_i \boldsymbol{\sigma}_i}{e}\right], \quad (2)$$

where the sum is over all particles (with cordinates r, θ, ϕ), each with an effective charge $e^{\lambda}_{eff_i}$, magnetic moment μ_i and mass m_i. As usual λ indicates the multipolarity, e is the electron charge.

In the present case the wave functions are not expressed in a single-particle proton or neutron basis, but rather in a two-cluster basis with the α (which is spinless) and either the triton or the helium-3. Therefore we cannot adopt the same simplifications as in ref. [21], but we have to rewrite the magnetic operator in a cluster form. For the dipole case this is not difficult and the magnetic operator can be recast in the form:

$$M(M1) = \sqrt{3}\boldsymbol{Y}_0 \times (\boldsymbol{\mu}_1 + \boldsymbol{\mu}_2 + \mu_N G\boldsymbol{L}) = \sqrt{3}\boldsymbol{Y}_0 \times(\mu_N G\boldsymbol{J} + (2\mu_{cl} - G)\boldsymbol{S}), \quad (3)$$

where the summation over the A particles has been simplified by partitioning the protons and neutrons into two spherical clusters (see appendix). Here $\boldsymbol{Y}$ indicates vector spherical harmonics, μ_1 and μ_2 are the intrinsic static magnetic operator of the clusters (in nuclear magnetons, μ_N) and $\boldsymbol{L} = \boldsymbol{J} - \boldsymbol{S}$ is the cluster-cluster orbital angular momentum operator. The total angular momentum and spin of the cluster are indicated with $\boldsymbol{J}$ and $\boldsymbol{S}$, respectively. The coefficient $G = \frac{Z_1 A_2^2 + Z_2 A_1^2}{A A_1 A_2}$ acts as an effective cluster-cluster orbital gyromagnetic factor. Since the α has null spin and null magnetic moment, only the intrinsic magnetic moment of the other cluster appears ($\mu_{cl} = \mu_2$).

By calculating the reduced matrix elements along the lines of ref. [21], one gets:

$$B(M1) = 9(2j_f+1)|\langle \ell_f j_f|\ell_i, j_i\rangle|^2 \langle \ell_f \|\boldsymbol{Y}_0\|\ell_i\rangle^2 \cdot \left[\mu_N G(-1)^{\ell_f + s_f + j_f - 1}\langle \ell_i j_i\|\boldsymbol{J}\|\ell_i, j_i\rangle \begin{Bmatrix} j_f & 1 & j_i \\ 1 & j_i & 0 \end{Bmatrix} \begin{Bmatrix} \ell_f & j_f & s_f \\ j_i & \ell_i & 0 \end{Bmatrix} \right.$$
$$\left. +(2\mu_{cl} - \mu_N G)\langle s_f||\boldsymbol{s}||s_i\rangle \begin{Bmatrix} \ell_f & s_f & j_f \\ \ell_i & s_i & j_i \\ 0 & 1 & 1 \end{Bmatrix}\right], \quad (4)$$

where ℓ_i, j_i, ℓ_f and j_f are the initial and final orbital and total angular momenta. The selection rule given by the overlap and the reduced matrix element of the vector spherical harmonic imply that one can only populate states with $\ell_i = \ell_f$ and $j_i \neq j_f$. In our specific case, where the initial state has $\ell_j = p_{3/2}$, we can only reach states with $p_{1/2}$ character. The corresponding $B(M1)$ is

$$B(M1) = \frac{1}{4\pi}(2\mu_{cl} - \mu_N G)^2 |\langle \ell_f j_f|\ell_i, j_i\rangle|^2 \quad (5)$$

that coincides to the formula given in refs. [1,3]. The calculation of the $B(M1; 3/2 \rightarrow 1/2)$ to the bound state (that is within the two isospin partner levels) gives an excellent agreement with experimental measurements as seen from table 2. Figure 3 shows continuum states excited in $M1$ transitions for ^{7}Be. Only transitions to the $p_{1/2}$ states are allowed because of orthogonality between the ground state $p_{3/2}$ and the continuum $p_{3/2}$ (see the next section for a more detailed discussion). The total non-energy weighted $B(M1)$ to the continuum states, integrated up to 50 MeV, is about 0.00408 μ^2, much smaller than the magnetic dipole strength to the first bound state.

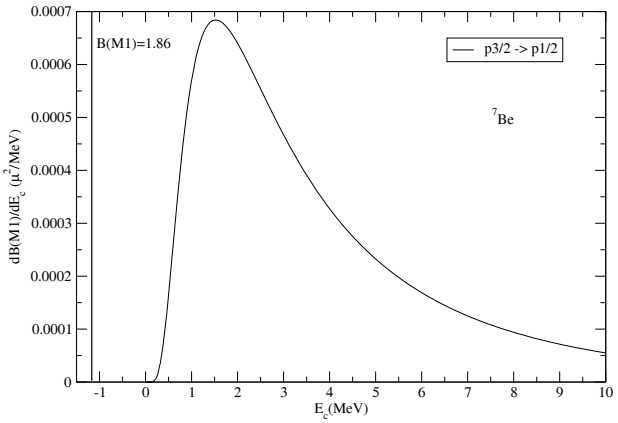

Fig. 3. Differential $\mathrm{d}B(M1)/\mathrm{d}E_c$ in μ^2/MeV for transitions from the ground state to the continuum. Energies are in MeV, referred to the threshold for breaking into the α-^{3}He channel.

1.2 ^{7}Li

In a previous paper [9] we have investigated dipole and quadrupole electric transitions of the nucleus ^{7}Li. We refer here to the same parameter sets for the potential and we improve our calculations by adding results for magnetic dipole transitions to the continuum for the sake of completeness. We note that ^{7}Li and ^{7}Be have the same qualitative behaviour because of their similar internal structure. An estimate of the static magnetic dipole moment of the ^{7}Li ground state obtained by using formula (A.9) gives $\mu(^7\mathrm{Li}) = 3.37\mu_N$ that is in good agreement with the experimental value $3.256\mu_N$ given in [22]. Again this fact confirms that in a simplified dicluster picture the $\ell = 1$ relative angular momentum gives a good magnetic dipole moment as in ^{7}Be.

^{7}Li and ^{7}Be have also the same qualitative behaviour with respect to transitions to the continuum: compare plots in ref. [9] with figs. 1 and 2 in the present paper and compare fig. 3 with fig. 4. In particular the last one shows the magnetic dipole transition strength for transitions between the ground state and the continuum. Only the transitions to $p_{1/2}$ continuum states are allowed because of orthogonality between the ground state $p_{3/2}$ and the $p_{3/2}$ continuum. This point was discussed, for another system, also in ref. [23].

The total integrated $B(M1)$ strength amounts to $0.0029\mu^2$ again much smaller than the $B(M1)$ to the first excited bound state. The magnetic dipole contribution is, in both nuclides, not as important as for the deuteron.

2 Molecular sum rules

Useful tools in nuclear physics are sum rules [24–27]. In particular energy-weighted sum rules (EWSM) for an electromagnetic interaction can be expressed in terms of proper expectation values in the ground state

$$S(\pi\lambda) \equiv \sum_f (E_f - E_i)B(\pi\lambda; i \rightarrow f) = \frac{1}{2}\langle 0|[\hat{O}(\pi\lambda), [H, \hat{O}(\pi\lambda)]]|0\rangle, \quad (6)$$

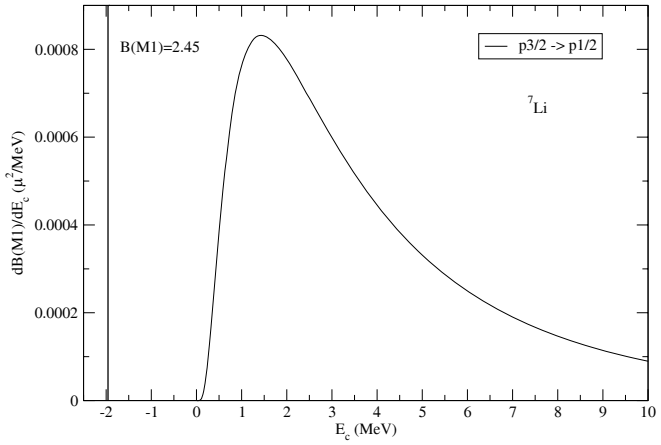

Fig. 4. Differential $\mathrm{d}B(M1)/\mathrm{d}E_c$ in μ^2/MeV for transitions from ground state to continuum. Energies are in MeV, referred to the threshold for breaking into the α-t channel.

where i stands for the initial state and the sum is extended over all reachable final states f. Here H is the Hamiltonian operator of the system. The energies of the initial and final states are E_i and E_f and the operator $\hat{O}(\pi\lambda)$ in the double commutator is the one that induces the transition. For electric dipole and quadrupole interactions, eq. (6) leads, respectively, to [24]:

$$S(E1) = \frac{9}{4\pi}\frac{\hbar^2}{2m}\frac{NZ}{A}e^2,$$
$$S(E2) = \frac{50}{4\pi}\frac{\hbar^2}{2m}Ze^2\langle r^2\rangle^{ch}. \quad (7)$$

where m is the nucleon mass and $\langle r^2\rangle^{ch}$ is the mean square charge radius. Our calculations show that the EWSR (7) are clearly not exhausted by considering only the transitions which imply changes in the relative motion (see table 3). We assume that the suitable sum rules in this case are the energy-weighted molecular sum rules (EWMSR) that can be obtained by removing the contributions of the individual clusters [25]. If a nucleus with mass and charge (A, Z) is split into two clusters (A_1, Z_1) and (A_2, Z_2) then the EWMSR is in general defined as

$$S_{mol}(E\lambda, A_1 + A_2) = S(E\lambda, A_1 + A_2) - S(E\lambda, A_1) - S(E\lambda, A_2). \quad (8)$$

For electric dipole [25] and quadrupole interactions one obtains:

$$S_{mol}(E1) = \frac{9}{4\pi}\frac{(Z_1A_2 - Z_2A_1)^2}{AA_1A_2}\frac{\hbar^2e^2}{2m},$$
$$S_{mol}(E2) = \frac{25}{4\pi}\left(Z_1\left(\frac{A_2}{A}\right)^2 + Z_2\left(\frac{A_1}{A}\right)^2\right)\langle R\rangle^2\frac{\hbar^2e^2}{m}.$$

The EWMSR for the quadrupole case is obtained by using formula (A.7) into eq. (8). Note that in ref. [25] the expectation value of $\langle R\rangle^2$ was approximated, in a phenomenological fashion, by the intercluster equilibrium distance, S_0.

Table 3. Comparison between EWSR, EWMSR and our calculations for ^{7}Li and ^{7}Be. Values are in MeV^2 fm^3 for $E1$, MeV^2 fm^5 for $E2$ and μ_N^2 MeV for $M1$.

	^{7}Li			^{7}Be		
$EM\lambda$	EWMSR	EWSR	ours	EWMSR	EWSR	ours
$E1$	1.02	36.7	1.01	1.02	36.7	1.00
$E2$	1120	2105	481.6	1424	3018	639
$M1$	1.36	–	1.20	0.87	–	0.82

Energy-weighted sum rules for the magnetic dipole [13] and higher multipolarities [14] have been evaluated in a pure single-particle scheme with a shell model Hamiltonian containing a spin-orbit part. The magnitude of the spin-orbit splitting is directly proportional to the total energy-weighted strength. In our cluster picture, one can follow a similar idea to evaluate the energy-weighted molecular sum rule for the magnetic dipole interaction. The model Hamiltonian is $\hat{H} = H_0 + V_{so}(R)\boldsymbol{L}\cdot\boldsymbol{S}$, where H_0 contains the kinetic term and the central part of the potential, while the operator that promotes magnetic dipole excitations amounts to the third component of $\hat{O} = \sum_{i=1,2}(G\boldsymbol{L}_i + 2\mu_i\boldsymbol{S}_i)$, where G (defined above and also in (A.9)) contains the combined effects of effective charges and reduced mass. The expectation value in the ground state of the double commutator gives

$$S_{mol}(M1, A_1 + A_2) = \frac{1}{2}\langle 0|[\hat{O}_z, [\hat{H}, \hat{O}_z]]|0\rangle = -\frac{1}{2}(G - 2\mu_2)^2\langle 0|V_{so}(R)\boldsymbol{L}\cdot\boldsymbol{S}|0\rangle. \quad (9)$$

We have calculated all the contributions of $E1$ and $E2$ transitions, including also the contribution of "virtual" states, or states that are not allowed by the Wildermuth rule ($0s_{1/2}, 1s_{1/2}, 0d_{5/2}, 0d_{3/2}$ for the electric dipole and $0p_{3/2}, 0p_{1/2}$ for the quadrupole). For the magnetic dipole interaction we have to consider the virtual state $0p_{1/2}$, the first excited state $1p_{1/2}$ and the continuum $p_{1/2}$, but we do not need to consider the virtual state $0p_{3/2}$. The reason is the following: in the reduced matrix element for an $M\lambda$ interaction the radial contribution is $\langle f|r^{\lambda-1}|i\rangle$. For the magnetic dipole interaction this contribution is simply the overlap between the initial state, i, and the final state, f. If the states carry the same angular momentum and spin quantum numbers then their overlap is zero by orthogonality, because they are different eigenstates of the same Hamiltonian (spin-orbit potential included). For the same reason the virtual state $0p_{1/2}$ does indeed contribute: since the spin-orbit part of the potential is different, the two Hamiltonians are different and one cannot use the property of orthogonality, but rather has to calculate the actual overlap.

In table 3 we compare EWSR and EWMSR with the values obtained in our model. We find that the low-lying dipole strength exhausts almost entirely the EWMSM, but represents only a small fraction of the EWSR. In the same way the quadrupole strength coming from changes in the

relative motion of dicluster configurations exhausts a large fraction of the EWMSR, but only a small part of the standard EWSR.

The energy-weighted molecular sum rule for magnetic dipole transitions is fulfilled quite well by our calculations: 88% in the case of lithium and 94% in the case of berillium. Practically all the contribution comes from the excitation to the first excited bound state.

3 Photo-dissociation and radiative capture

The knowledge of the electromagnetic response to continuum is a basic ingredient to describe break-up processes. In fact, in kinematic conditions where the process is dominated by the Coulomb interaction (for example at very forward angles), the break-up probabilities become directly proportional to the $B(E\lambda)$ values. Independently of kinematic conditions this is also the case for two other processes of fundamental importance for astrophysics that can be therefore studied within the present model: the photo-dissociation and its inverse process, the radiative capture.

The electric and magnetic response functions obtained so far can be used to calculate the cross-sections for these two processes. The radiative-capture cross-section for type (π = electric or magnetic) and multipolarity λ, can be expressed [18] as

$$\sigma_{capt}(\pi\lambda, E_c) = \frac{2(2j+1)}{(2j_\alpha+1)(2j_{cl}+1)} \left(\frac{k_\gamma}{k_{\alpha\text{-}cl}}\right)^2 \times \sigma_{ph.dis}(\pi\lambda, E_c), \tag{10}$$

where $k_{\alpha\text{-}cl}$ is the wave number for the relative motion of the two clusters (one is always an α particle in the present case) and $\frac{2(2j+1)}{(2j_\alpha+1)(2j_{cl}+1)}$ is a spin factor from the detailed balance principle. This expression relies on the knowledge of the photo-dissociation cross-section that may be expressed as follows:

$$\sigma_{ph.dis}(\pi\lambda, E_c) = (2\pi)^3 \frac{(\lambda+1)}{[\lambda(2\lambda+1)!!]^2} k_\gamma^{2\lambda-1} \frac{\mathrm{d}B(\pi\lambda, E_c)}{\mathrm{d}E_c}, \tag{11}$$

where $\frac{\mathrm{d}B(\pi\lambda,E_c)}{\mathrm{d}E_c}$ is the reduced transition probability (defined as in ref. [18]), k_γ is the photon wave number, λ is the multipolarity of the transition, $E_c = \hbar^2 k^2_{\alpha\text{-}cl}/2\mu_r$ is the relative energy of the two clusters in the continuum and $E_\gamma = E_c + E_b$ is the photon energy. Here we have used the notation μ_r for the reduced mass and E_b for the binding energy.

To evaluate the total photo-dissociation cross-section, starting from a given bound state, one has to sum over all possible angular-momentum transfer and possible allowed spins of the final states in the continuum. In the calculation of the total capture cross-section, in addition, one has to include all the bound states.

Figure 5 shows a schematic picture for the two processes (left side), and the respective cross-sections (right side). They are very similar at a qualitative level, but the different binding energies of the ground states (mostly due to the different charge) makes up for changes in the position of the resonances and in the intensity of the transition to the low-lying continuum.

This is evident from the comparison of fig. 1 of the present paper and fig. 1 of our older work on ^{7}Li [9]. The $BE(1)$ to low-lying continuum states has a slightly different contribution from the s and d states that explains the differences in the cross-section at small energies. Indeed it is known that the shape and position of the maxima in the response are affected by the binding energy, initial and final angular momenta and Coulomb barrier height [18,28].

The electric dipole clearly dominates the cross-section, although the electric quadrupole shows peaks due to the presence of two low-lying resonances. The electric quadrupole and the magnetic dipole are of comparable size and are nevertheless not negligibly small in comparison with the other contributions.

The photo-dissociation cross-section is shown only from the ground state, but the radiative capture can go directly to the ground state or proceed through the first excited bound state. In the latter case, due to the small energy difference, the cross-sections to the $p_{1/2}$ and $p_{3/2}$ are practically proportional and the proportionality is fixed by the phase space factor depending on the total spin, j.

4 S-factors

In the stellar environment the occurrence of high temperatures and the large density of light isotopes makes the α-capture a very likely process. Tritium and ^{3}He participate in (α,γ) reactions forming mass $A = 7$ isobars, which are one possible getaway toward heavier nuclei. It is therefore important to understand well these processes and to have simple models to treat the reactions. Once again the dicluster picture qualitatively and quantitatively entails the correct physics ingredients: indeed the astrophysical S-factor (a reparameterization of the cross-section, defined by $S = e_{rel}\sigma_{capt}(e_{rel})e^{2\pi\eta}$, where η is the Sommerfeld parameter) for the reaction $^3\mathrm{He}(\alpha,\gamma)^7\mathrm{Be}$ is reasonably well reproduced, as can be seen in figs. 6. Good results are also obtained for the partner reaction, $^3\mathrm{H}(\alpha,\gamma)^7\mathrm{Li}$, as shown in fig. 7. Each curve has both a positive and a negative aspect: while the result for Be has a good magnitude, but a non-optimal slope, the result for Li has a good shape, but it overestimates the data. Our results do not contain any rescaling of the S-factor or, in other words, we assume a spectroscopic factor for the α+cluster configuration equal to one. This might be the reason for the observed deviation in the case of ^{7}Li, where the $^6\mathrm{Li} + \mathrm{n}$ component may affect the total magnitude although possibly not the overall shape. The reason for the flat shape of the ^{7}Be curve might also reside in the prescription we have used to treat the dicluster system. Perhaps it is an indication that other components are affecting the properties at low energies although the results in table 2 were very satisfactory.

The various sets of experimental measurements that are reported in these figures together with the calculated values, are taken from the NACRE database [29], where

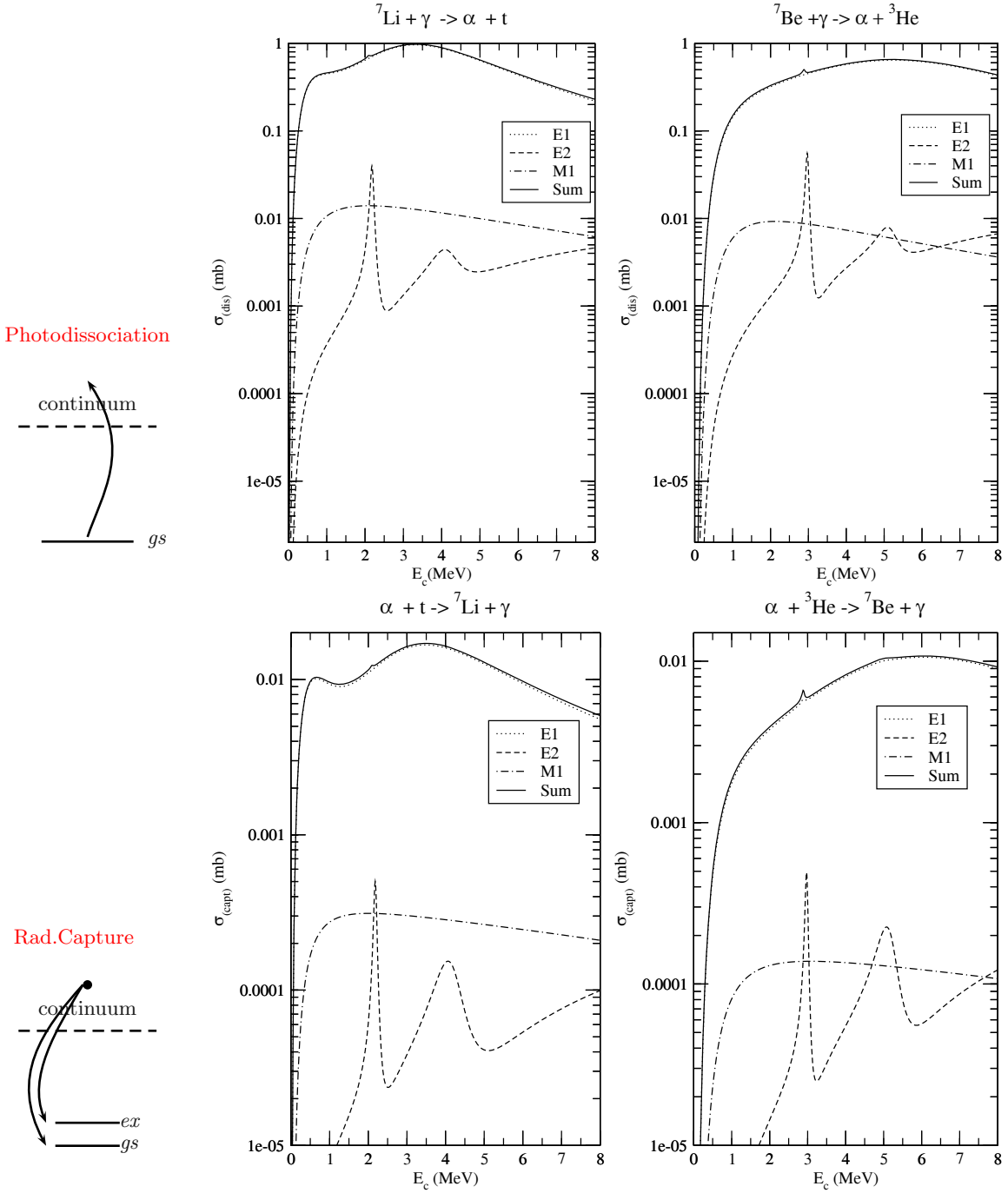

Fig. 5. Photo-dissociation and radiative-capture processes (left) and cross-sections (right) plotted against the continuum energy for reactions involving ^{7}Li and ^{7}Be. The $E1$, $E2$ and $M1$ contributions are shown separately and the total practically coincides with the electric dipole contribution. The $E2$-resonances are seen in each picture. The photo-dissociation is shown only from the ground state, but the radiative capture can go directly to the ground state or proceed through the first excited state.

an extensive list of references can be found. A simple parabolic fit of the model curves give a $S(0)$ of 0.42 and 0.13 keV b for beryllium and lithium, respectively.

Other more refined approaches, like the R-matrix calculations (see the discussion in ref. [12]), or the multichannel algebraic scattering approach [11] have been applied with success to the same reaction. Although our model is much simpler than the cited approaches, it has a comparable predictive power. Of course this might still not be enough for elaborated nucleosynthesis models that must consider a network of nuclear reactions with very precise fits. In that case a more precise determination of the S-factor might be necessary and one must go beyond the simple cluster picture.

The whole idea of parametrizing the capture cross-section in terms of the S-factors is precisely to smooth

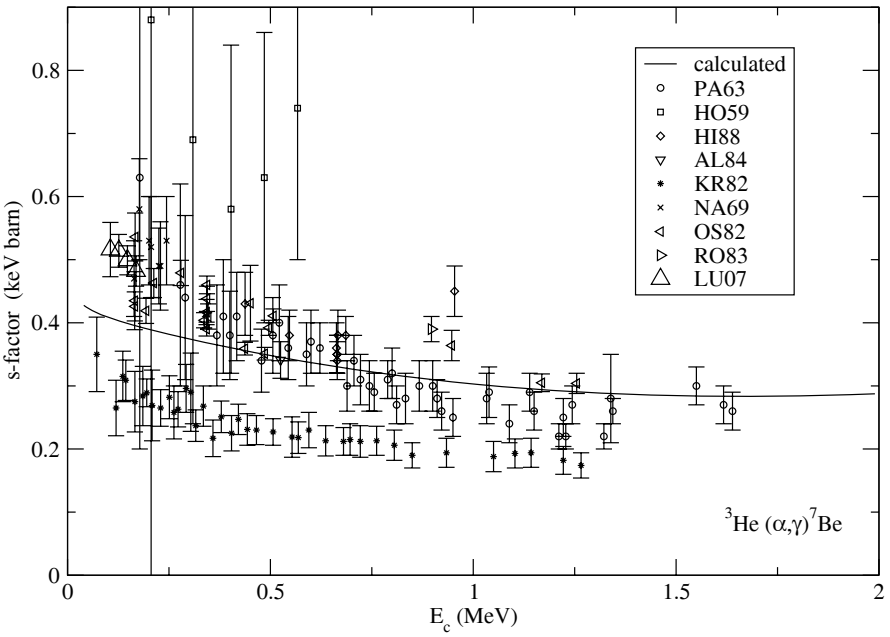

Fig. 6. S-factor for the $^3\mathrm{He}(\alpha,\gamma)^7\mathrm{Be}$ reaction.

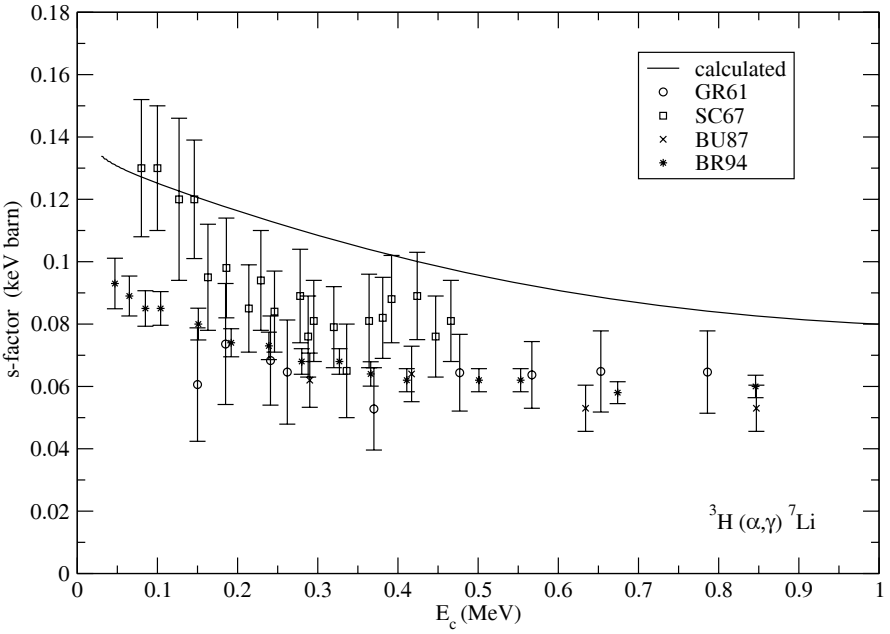

Fig. 7. S-factor for the $^3\mathrm{H}(\alpha,\gamma)^7\mathrm{Li}$ reaction.

out the effects of the Coulomb interaction [30] (by means of the exponential term containing the Sommerfeld parameter). The important effect of the nuclear interaction in the low-energy regime can be seen in fig. 8 and cannot be neglected. The upper panel displays the integrand of the response function as a function of r for a given energy of $E_c = 50\,\mathrm{keV}$ in the continuum. We have selected the $s_{1/2} \rightarrow p_{3/2}$ transition in ^{7}Be for the sake of simplicity. Clearly the nuclear potential does not affect the tail of the wave function, that matches a pure Coulomb wave function at large distances, but at distances smaller than the position of the Coulomb barrier, the presence of the nuclear potential affects the continuum wave functions and therefore the response in the continuum. The S-factor, in the low-energy regime, is displayed in the lower panel. The nuclear potential is seen to lower the S-factor significantly and cannot be excluded from calculations, as already found by several authors.

5 Conclusions

An elementary dicluster model is found to provide an effective description of static as well as dynamic properties

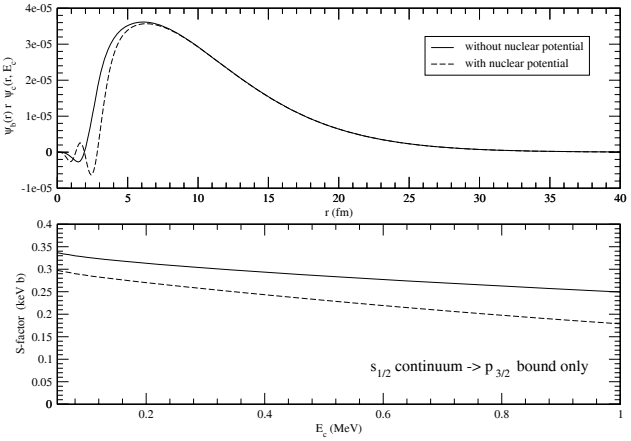

Fig. 8. Integrand of the response function for the transition $s_{1/2} \rightarrow p_{3/2}$ in ^{7}Be for a given energy $E_c = 50\,\mathrm{keV}$ (upper panel) and S-factor for the same transition in the low-energy regime (lower panel). The two curves are calculated including (dashed) or excluding (solid) the nuclear potential in the evaluation of the continuum wave function.

of some light nuclei and can be used with confidence in reaction models. Although *ab initio* many-body models are expected to provide better results in the general case, we have shown that, for example, the astrophysical S-factor, which is a crucial quantity for interdisciplinary applications of nuclear physics, is reasonably well reproduced by the dicluster model.

In particular we have investigated the magnetic properties of $A = 7$ isobars, introducing a new molecular magnetic dipole sum rule, that has a close analogy with the single-particle magnetic sum rule [14], and finding that (as expected) the contribution to photo-dissociation and radiative-capture processes is rather small. This is in contrast with the strong $M1$ photo-dissociation peak at low energies in the case of deuteron, that has motivated our investigation.

Appendix A. Derivation of standard formulae for dicluster nuclei

We summarize here a few important formulae valid for dicluster nuclei [1,16]. They are often used in the literature, but the derivation, albeit elementary in some cases, is rarely reported.

Matter radius

The mean square matter radius of a nucleus with mass number A is defined as

$$r^2 = \frac{\sum_{i=1}^{A} \boldsymbol{r}_i{}^2}{A}\,. \tag{A.1}$$

Assuming that the nucleus made up by two clusters with mass number A_1, A_2 and $A = A_1 + A_2$, eq. (A.1) becomes

$$r_A^2 = \frac{\sum_{i=1}^{A_1}(\boldsymbol{R}_{A_1} + \boldsymbol{R}_i)^2 + \sum_{j=1}^{A_2}(\boldsymbol{R}_{A_2} + \boldsymbol{R}_j)^2}{A}\,, \tag{A.2}$$

where $\boldsymbol{R}_{i,j}$ are position vectors measured from the center of mass of each cluster, $A_{1,2}$, respectively; $\boldsymbol{R}$ is the inter-cluster distance that can be split into two vectors, $\boldsymbol{R}_{A_1}$ and $\boldsymbol{R}_{A_2}$ related by

$$\begin{aligned} \boldsymbol{R}_{A_1} &= -\frac{A_2}{A}\boldsymbol{R}, \\ \boldsymbol{R}_{A_2} &= \frac{A_1}{A}\boldsymbol{R}. \end{aligned} \tag{A.3}$$

By inserting (A.3) in (A.2) and upon taking the expectation values rather than the operators, one gets

$$\langle r^2\rangle_{A_1+A_2} = \frac{A_1}{A}\langle r^2\rangle_{A_1} + \frac{A_2}{A}\langle r^2\rangle_{A_2} + \frac{A_1A_2}{(A)^2}\langle R^2\rangle. \tag{A.4}$$

Charge radius

The mean square charge radius of a nucleus with atomic number Z is

$$r_{ch}^2 = \frac{\sum_{i=1}^{Z} \boldsymbol{r}_i{}^2}{Z}\,. \tag{A.5}$$

For a nucleus composed by two clusters with atomic numbers Z_1, Z_2 and $Z = Z_1 + Z_2$ eq. (A.5) becomes

$$r_{ch}^2 = \frac{\sum_{i=1}^{Z_1}(\boldsymbol{R}_{A_1} + \boldsymbol{R}_i)^2 + \sum_{i=1}^{A_2}(\boldsymbol{R}_{A_2} + \boldsymbol{R}_i)^2}{Z}\,. \tag{A.6}$$

Using (A.3) and taking the expectation values of operators, one finds

$$\begin{aligned} \langle r^2\rangle^{ch}_{A_1+A_2} = {} & \frac{Z_1}{Z}\langle r^2\rangle^{ch}_{A_1} + \frac{Z_2}{Z}\langle r^2\rangle^{ch}_{A_2} \\ & + \frac{\langle R^2\rangle}{Z}\left(Z_1\cdot\left(\frac{A_2}{A}\right)^2 + Z_2\cdot\left(\frac{A_1}{A}\right)^2\right). \end{aligned} \tag{A.7}$$

Magnetic dipole moment

The magnetic dipole moment operator is defined as

$$\boldsymbol{\mu} = \sum_{i=1}^{A+B}\mu_i = \sum_{i=1}^{A+B}\left(g_i^\ell\boldsymbol{\ell}_i + g_i^s\boldsymbol{s}_i\right)\mu_N \tag{A.8}$$

with $g^\ell = 1$ for protons, $g^\ell = 0$ for neutrons, $g^s = 5.58$ for protons and $g^s = -3.83$ for neutrons. The orbital angular momenta are defined as $\boldsymbol{\ell}_i = \boldsymbol{r}_i \times \boldsymbol{p}_i$, where $\boldsymbol{r}_i = \boldsymbol{R}_{A_1} + \boldsymbol{R}_i$ for cluster A_1 and $\boldsymbol{r}_j = \boldsymbol{R}_{A_2} + \boldsymbol{R}_j$ for cluster A_2. The same rule can be applied to momenta $\boldsymbol{p}_i$. Labelling with $\boldsymbol{\mu}_1, \boldsymbol{\mu}_2$ the intrinsic magnetic dipole moments of each of the two clusters, (A.8) becomes

$$\boldsymbol{\mu} = \boldsymbol{\mu}_1 + \boldsymbol{\mu}_2 + \mu_N \underbrace{\frac{Z_1A_2^2 + Z_2A_1^2}{AA_1A_2}}_{G}\boldsymbol{L}\,, \tag{A.9}$$

where one has isolated in the third term the contribution from the relative orbital angular momentum, $\boldsymbol{L}$. The total magnetic moment is therefore simply the sum of the magnetic moments of the two subsystems plus the contribution from the cluster-cluster orbital motion, which vanishes if the two cluster are in a relative s-state.

Matter and charge quadrupole moments

Matter and charge quadrupole operators moments are defined as

$$Q^{mat} = \sum_{i=1}^{A_1+A_2} r_i^2 Y_{20}(\theta_i, \phi_i), \tag{A.10}$$

$$Q^{ch} = \sum_{i=1}^{A_1+A_2} e_i r_i^2 Y_{20}(\theta_i, \phi_i) \tag{A.11}$$

and, by using the definition of the spherical harmonic and by splitting the sums over the total nucleon number into two sums over the nucleons of each cluster, we obtain two relationships that contain the intrinsic quadrupole moments of the clusters and a term that expresses the quadrupole operator for the relative motion, namely:

$$Q^{mat} = Q^{mat}_{A_1} + Q^{mat}_{A_2} + \frac{A_1 A_2^2 + A_2 A_1^2}{A^2} R^2 Y_{20}(\Theta, \Phi),$$

$$Q^{ch} = Q^{ch}_{A_1} + Q^{ch}_{A_2} + \frac{Z_1 A_2^2 + Z_2 A_1^2}{A^2} R^2 Y_{20}(\Theta, \Phi). \tag{A.12}$$

With these operators one can calculate the quadrupole moments by evaluating the expectation value in the ground state with the maximally aligned magnetic substate:

$$Q^{mo} = \sqrt{\frac{16\pi}{5}} \langle L, M = L | Q | L, M = L \rangle. \tag{A.13}$$

For example in the case of the matter quadrupole moment one has:

$$Q^{mat.mo} = Q^{mat.mo}_{A_1} + Q^{mat.mo}_{A_2} + \frac{A_1 A_2^2 + A_2 A_1^2}{A^2} \times \langle R^2 \rangle 2(2L+1)(-1)^L \begin{pmatrix} L & 2 & L \\ -L & 0 & L \end{pmatrix} \begin{pmatrix} L & 2 & L \\ 0 & 0 & 0 \end{pmatrix}, \tag{A.14}$$

where L is the angular momentum of the relative motion. In the case of the two mirror isobars lithium and beryllium, we have $L = 1$ and therefore the above formula reduces to

$$Q^{mat.mo} = Q^{mat.mo}_{A_1} + Q^{mat.mo}_{A_2} - \frac{2}{5} \frac{A_1 A_2^2 + A_2 A_1^2}{A^2} \langle R^2 \rangle. \tag{A.15}$$

Analogous expressions may be derived for the charge quadrupole moments that differ only in the coefficient that depends linearly on charges rather than masses. Notice also that, while the coefficient of the relative motion part for the charge quadrupole moment is different for lithium and beryllium, the one for the matter quadrupole moment is the same. Another difference comes from the average square radius of the relative motion wave function, which is not identical for the two nuclei.

References

1. H. Walliser, T. Fliessbach, Phys. Rev. C **31**, 2242 (1985).
2. K. Wildermuth, Y.C. Tang, *A Unified Theory of the Nucleus* (Academic Press, New York, 1977).
3. B. Buck, R.A. Baldock, J. Alberto-Rubio, J. Phys. G: Nucl. Phys. **11**, L11 (1985).
4. T. Kajino, A. Arima, Phys. Rev. Lett. **52**, 739 (1984).
5. T. Kajino, Nucl. Phys. A **460**, 559 (1986).
6. T. Kajino *et al.*, Phys. Rev. C **37**, 512 (1988).
7. T. Altmeyer, Z. Phys. A **330**, 277 (1988).
8. K. Langanke, Nucl. Phys. A **457**, 351 (1986).
9. L. Fortunato, A. Vitturi, Eur. Phys. J. A **26**, 33 (2005).
10. K. Nollett, Phys. Rev. C **63**, 054002 (2001).
11. L. Canton, L.G. Levchuk, arXiv:0805.2667v2 [nucl-th].
12. Gy. Gyürky *et al.*, Phys. Rev. C **75**, 035805 (2007); F. Confortola *et al.*, Phys. Rev. C **75**, 065803 (2007); Gy. Gyürky *et al.*, J. Phys. G: Nucl. Part. **35**, 014002 (2008).
13. D. Kurath, Phys. Rev. **130**, 1525 (1963).
14. M. Traini, Phys. Rev. Lett. **41**, 1535 (1978).
15. I. Tanihata *et al.*, Phys. Rev. Lett. **55**, 2676 (1985).
16. H. Walliser, Q.K.K. Liu, Y.C. Tang, Phys. Rev. C **28**, 57 (1983).
17. X. Hu, D.R. Tilley, J.H. Kelley, J.L. Godwin *et al.*, Nucl. Phys. A **708**, 3 (2002) and corrections in D.R. Tilley *et al.*, TUNL manuscript.
18. S. Typel, G. Baur, Nucl. Phys. A **759**, 247 (2005); G. Baur, S. Typel, Prog. Part. Nucl. Phys. **59**, 122 (2007).
19. F. Catara, C.H. Dasso, A. Vitturi, Nucl. Phys. A **602**, 181 (1996).
20. J.M. Blatt, V.F. Weisskopf, *Theoretical Nuclear Physics* (John Wiley and Sons, Inc., 1952).
21. A. De Shalit, I. Talmi, *Nuclear Shell Theory* (Academic Press, New York and London, 1963).
22. F. Ajzenberg-Selove, Nucl. Phys. A **413**, 1 (1984).
23. D. Krolle *et al.*, Z. Phys. A **328**, 291 (1987).
24. A. Bohr, B.R. Mottelson, *Nuclear Structure* (W.A. Benjamin, Inc., New York, Amsterdam, 1969).
25. Y. Alhassid, M. Gai, G.F. Bertsch, Phys. Rev. Lett. **49**, 1482 (1982).
26. H.J. Assenbaum, K. Langanke, A. Weiguny, Phys. Rev. C **35**, 755 (1987).
27. C.A. Bertulani, A. Sustich, Phys. Rev. C **46**, 2340 (1992).
28. M.A. Nagarajan, S.M. Lenzi, A. Vitturi, Eur. Phys. J. A **24**, 63 (2005).
29. NACRE database, `http://pntpm.ulb.ac.be/Nacre/nacre_d.htm`.
30. C.E. Rolfs, W.S. Rodney, *Cauldrons in the Cosmos* (University of Chigaco Press, 1988).